Hamiltonian of the $S = \frac{1}{2}$ dimerized antiferromagnetic-ferromagnetic quantum spin chain $BaCu_2V_2O_8$

E. S. Klyushina,[1,2,*] A. T. M. N. Islam,[1] J. T. Park,[3] E. A. Goremychkin,[4,†] E. Wheeler,[5] B. Klemke,[1] and B. Lake[1,2]

[1]*Helmholtz-Zentrum Berlin für Materialien und Energie, 14109 Berlin, Germany*

[2]*Institut für Festkörperphysik, Technische Universität Berlin, 10623 Berlin, Germany*

[3]*Heinz Maier-Leibnitz Zentrum, TU München, 85747 Garching, Germany*

[4]*Rutherford Appleton Laboratory, Chilton, Didcot, Oxon OX11 0QX, United Kingdom*

[5]*Institut Laue-Langevin, Boite Postale 156X, F-38042 Grenoble Cedex 9, France*

(Received 6 July 2018; published 12 September 2018)

The novel quantum magnet $BaCu_2V_2O_8$ was recently discovered to be a rare physical realization of a one-dimensional antiferromagnetic-ferromagnetic dimerized chain which displays strongly correlated phenomena at elevated temperatures [E. S. Klyushina *et al.*, Phys. Rev. B **93**, 241109(R) (2016)]. This paper presents an extended study of the Hamiltonian of $BaCu_2V_2O_8$ at base temperature. Static susceptibility and inelastic neutron scattering data are compared to several theoretical models. An analytical relation for the dynamic structure factor of the complex unit cell of $BaCu_2V_2O_8$ is derived and used to identify the intrachain exchange paths. Further analysis using the first moment of the dynamic structure factor was employed to determine the exchange path responsible for the intradimer interaction. This analysis reveals that the dimer chain is formed by a dominant antiferromagnetic exchange interaction $J_{\text{intra}} = 40.92$ meV which is realized via the Cu-O-V(II)-O-Cu superexchange path and a weak ferromagnetic coupling $J_{\text{inter}} = -11.97$ meV which arises within the copper-oxygen double plaquettes.

DOI: 10.1103/PhysRevB.98.104413

I. INTRODUCTION

Dimerized quantum magnets have attracted considerable attention in the last decades since extraordinary quantum phenomena such as bound and multimagnon states [1], Bose-Einstein condensation [2], and strongly correlated behavior at finite temperatures [3–5] were discovered in these systems.

In the dimerized magnetic system, spin-half magnetic ions are strongly coupled by the antiferromagnetic (AFM) exchange interaction into pairs known as *dimers*. These *dimers* are characterized by a spin-singlet nonmagnetic ground state and degenerate $S - 1$ triplet excitations which are gapped. The excitations are called magnons or *triplons* and are restricted by the hard-core constraint which allows only one excitation per dimer site [6]. *Dimers* interact with each other via this hard-core repulsion [3] and via weak interdimer exchange interactions which couple them in one-, two-, or three-dimensional structures.

In one-dimensional (1D) dimerized quantum magnets the strong intradimer magnetic exchange interaction J_{intra} alternates with a weaker interdimer magnetic exchange coupling J_{inter} along one particular direction within the crystal lattice so that the dimers form dimerized chains. The Hamiltonian of the dimerized chain is [7]

$$H = J_{\text{intra}} \sum_{i=1} \vec{S}_{2i-1} \cdot \vec{S}_{2i} + \alpha \vec{S}_{2i} \cdot \vec{S}_{2i+1}, \qquad (1)$$

where $\vec{S}_{2i}$ is the spin of the magnetic ion at the $2i$ crystal site and $\alpha = J_{\text{inter}}/J_{\text{intra}}$ is the dimerization ratio; the positive sign of J_{inter} and J_{intra} defines an AFM interaction and a negative sign a ferromagnetic (FM) interaction.

Dimerized chains are particularly interesting because they can develop strongly correlated behavior at finite temperatures which is caused by strong interactions between the excitations via the interdimer exchange coupling and the hard-core repulsion [10]. The strongly correlated phenomena manifest themselves as an asymmetric Lorentzian thermal line-shape broadening of the magnetic excitations and were first observed in the AFM-AFM dimerized chain compound copper nitrate [3,11]. These phenomena are not limited to 1D systems and were detected more recently in the three-dimensional (3D) dimerized antiferromagnet $Sr_3Cr_2O_8$ [4,5].

Although dimerized quantum antiferromagnets have been intensively studied, dimerized magnetic systems which have ferromagnetic interdimer exchange coupling have not been well explored. This is because physical realizations of AFM-FM dimerized quantum magnets are very rare, and in most cases their Hamiltonians have not been accurately determined via inelastic neutron scattering. Indeed, only a few inorganic compounds [12–14] have been suggested as physical realizations of the $S = \frac{1}{2}$ AFM-FM dimerized spin chain, while the larger number of proposed organic complexes are less suitable for inelastic neutron scattering and have been mainly studied by measuring their thermodynamic properties [15–18] apart from rare exceptions, e.g., Ref. [19].

In this paper, we investigate in detail the Hamiltonian of the novel compound $BaCu_2V_2O_8$, which we recently discovered to be a dimerized AFM-FM chain with a high magnetic energy scale and which displays strongly correlated behavior

*Corresponding author: ekaterina.klyushina@helmholtz-berlin.de

†Present address: Frank Laboratory of Neutron Physics, Joint Institute for Nuclear Research, Dubna, Moscow Region, 141980, Russia.

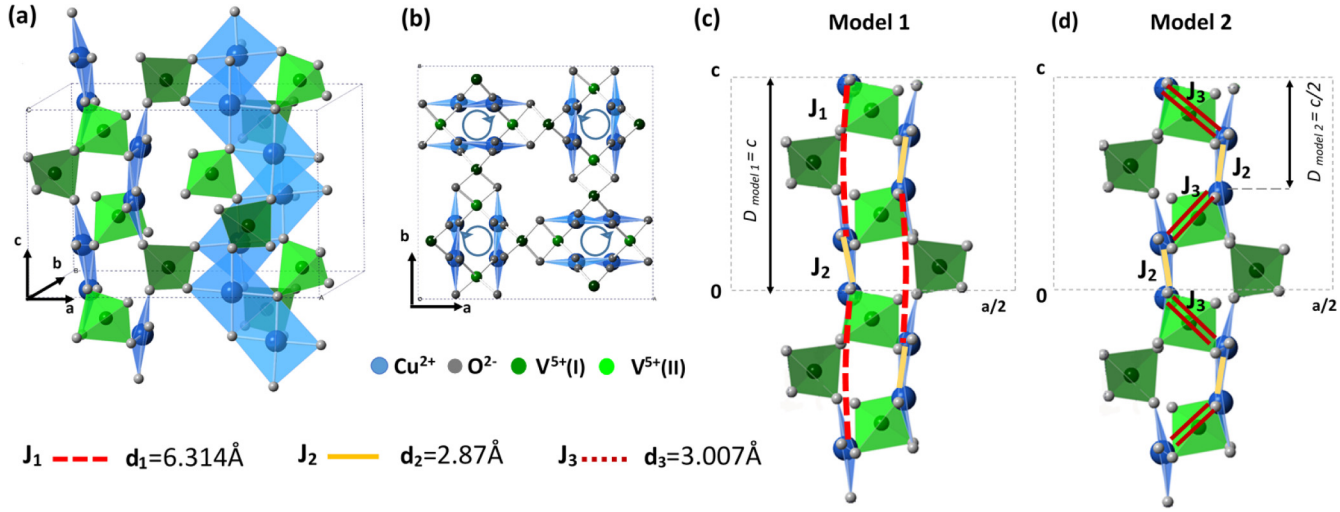

FIG. 1. (a) The crystal structure of $BaCu_2V_2O_8$. For clarity, only two of the four chains are shown and the Ba^{2+} ions are omitted. The blue and gray filled circles represent the magnetic Cu^{2+} ions and oxygen O^{2-} anions, respectively. The dark and light green filled circles are the nonmagnetic V^{5+}(I) and V^{5+}(II) vanadium ions which have different crystallographic sites, respectively. The dashed gray lines give the borders of the unit cell. (b) Projection of the crystal structure of $BaCu_2V_2O_8$ on the *ab* plane where the blue circles indicate the direction of rotation of the screw chains along the *c* axis. (c), (d) Models 1 and 2 for the magnetic exchange paths in $BaCu_2V_2O_8$ discussed in the text and suggested (c) by He *et al.* [8] and (d) by Koo *et al.* [9], respectively. The dashed red, solid yellow, and double red lines represent the Cu-O-V(I)-O-Cu (J_1), Cu-O-Cu (J_2), and Cu-O-V(II)-O-Cu (J_3) magnetic exchange paths, respectively. d_1, d_2, and d_3 give the direct distances between the magnetic Cu^{2+} ions in the exchange paths J_1, J_2, and J_3. The $D_{\text{model 1}}$ and $D_{\text{model 2}}$ give the dimer periodicity for *model 1* [8] and *model 2* [9].

at elevated temperatures [20] similar to that observed in several other dimerized compounds [3–5,11]. $BaCu_2V_2O_8$ is particularly interesting because its magnetic excitations retain their coherence up to $T = 250$ K which is much higher than the temperatures reported for other dimerized compounds where strongly correlated behavior was also observed [3–5,11]. This makes $BaCu_2V_2O_8$ a model compound and detailed knowledge of its Hamiltonian is important for a better understanding of its magnetic properties.

$BaCu_2V_2O_8$ has a tetragonal crystal structure with the space group $I\bar{4}2d$ (lattice parameters $a = b = 12.744$ Å, $c = 8.148$ Å) [21] where the $S = \frac{1}{2}$ magnetic Cu^{2+} ions are coordinated by O^{2-} and form square-planar CuO_4 plaquettes (Fig. 1). These CuO_4 plaquettes are paired into edge-sharing Cu_2O_6 double plaquettes. These double plaquettes are connected to each other via VO_4 tetrahedra with nonmagnetic V^{5+} ions, and form twofold screw chains along the *c* axis [Fig. 1(a)].

The *c* axis always lies within the Cu_2O_6 double plaquettes which rotate about it by 180°. There are four screw chains within each unit cell, two which are left handed and two are right handed where the left-handed screw chains are rotated by 90° with respect to the right-handed screw chains [Fig. 1(b)].

The magnetic models of $BaCu_2V_2O_8$ proposed in the literature vary from the dimerized AFM chains [8,9] to isolated AFM dimers [22]. First, He *et al.* [8] suggested that $BaCu_2V_2O_8$ consists of noninteracting pairs of linear dimerized chains which arise along the *c* axis via the dominant AFM superexchange path Cu-O-V(I)-O-Cu (path J_1) and a weaker AFM superexchange path Cu-O-Cu (path J_2) within the edge-sharing double plaquettes [Fig. 1(c)]. In this model, each crystallographic screw chain gives rise to one pair of linear magnetic chains, and each magnetic chain has one dimer per *c*-lattice parameter. We call this *model 1*. The values of the energy gap (Δ), dominant intradimer exchange coupling (J_{intra}), and dimerization ratio (α) were estimated to be $\Delta = 230$ K, $J_{\text{intra}} = 260$ K, and $\alpha = 0.2$ from the analysis of powder dc magnetic susceptibility data. Later, the results of ^{51}V nuclear magnetic resonance measurements [23] suggested that $\Delta = 450$–470 K within the same model which is consistent with the value obtained by He *et al.* [8]. The factor of 2 between these results is due to the fact that He *et al.* used a Hamiltonian whose parameters are rescaled by 2 compared to Eq. (1).

Another model was developed by Koo *et al.* [9] and based on the results of extended Hückel tight-binding calculations. They suggested that $BaCu_2V_2O_8$ consists of dimerized AFM chains which run along the *c* axis, but in contrast to the first model, these chains are not straight but are in fact the screw chains evident in the crystal structure with two dimers per *c*-lattice parameter [Fig. 1(d)]. We call this *model 2*. The calculations predicted a dominant AFM superexchange path Cu-O-V(II)-O-Cu (path J_3) and a weaker AFM path J_2. The dimerization ratio is estimated to be $\alpha = 0.164$ assuming *a priori* that the magnetic exchange constants are AFM.

First principles electronic structure (FPES) calculations [22] also predicted that J_{intra} and J_{inter} are realized via the AFM J_2 and J_3 paths, respectively, supporting the screw AFM dimerized chain (model 2) suggested by Koo *et al.*. However, the FPES calculations estimated the dimerization ratio to be $\alpha = 0.05$ which is much smaller than $\alpha = 0.164$ calculated using the Hückel tight-binding approach. Thus, according to the FPES calculations, $BaCu_2V_2O_8$ can be viewed as an isolated dimer system rather than a dimerized chain [22].

We recently explored the magnetic excitation spectra of $BaCu_2V_2O_8$ at base temperature and compared them to the results of state-of-the-art numerical computations performed using the density-matrix renormalization group (DMRG) tech-

nique [20]. This comparison revealed that $BaCu_2V_2O_8$ is a AFM-FM screw chain where the AFM dimers are coupled by weak *ferromagnetic* interdimer interactions along the *c* axis. This is in contrast to all previous results [8,9,22] which suggest that all interactions in $BaCu_2V_2O_8$ are AFM. Although the Hamiltonian of $BaCu_2V_2O_8$ was solved, the magnetic exchange path responsible for the dominant AFM coupling was not identified nor was the relation for the complex dynamic structure factor observed experimentally at base temperature derived analytically.

This paper presents a detailed investigation of the Hamiltonian of $BaCu_2V_2O_8$ using static magnetic susceptibility and inelastic neutron scattering (INS) measurements whose results were analyzed (i) to identify the dominant magnetic exchange path and (ii) to introduce the analytical relation for the complex dynamic structure factor of $BaCu_2V_2O_8$ observed experimentally at base temperature.

The paper is organized as follows. First, we carefully explore the static susceptibility and magnetic excitation spectra of $BaCu_2V_2O_8$ to solve the Hamiltonian of this compound. After that, we derived the analytical relation for the dynamic structure factor of the dimerized screw chain which allows the complex magnetic excitation spectrum of $BaCu_2V_2O_8$ to be computed using the extracted Hamiltonian. Finally, we analyze the intensity distribution of the magnetic excitation spectra of $BaCu_2V_2O_8$ using the relation for the first moment of the dynamic structure factor to identify the dominant AFM exchange path.

In this paper, we prove that $BaCu_2V_2O_8$ is a dimerized 1D AFM-FM system where the AFM dimers are weakly bounded ferromagnetically via the Cu-O-Cu magnetic exchange path to form screw chains along the *c* axis.

II. EXPERIMENTAL DETAILS

Powder and single-crystalline samples of $BaCu_2V_2O_8$ were grown in the Core Lab for Quantum Materials at the Helmholtz Zentrum Berlin fur Materialien und Energie (HZB) in Germany. The polycrystalline powder sample and feed rod for single-crystal growth of $BaCu_2V_2O_8$ were both prepared by standard solid-state reactions using high-purity powders of $BaCO_3$ (99.997%, Alfa Aesar), CuO (99.995%,Alfa Aesar), and V_2O_5 (99.99%, Alfa Aesar). After mixing thoroughly in ethanol, in the 1:2:1 molar ratio, powder of stoichiometric composition was sintered in air at 650 °C twice for 12 h with intermediate grinding. The powder was then packed in a rubber balloon and pressed hydrostatically up to 3000 bars in a cold-isostatic-pressure machine and sintered in air at 750 °C for 12 h to form a dense cylindrical rod of about 6 mm in diameter and about 7 cm in length.

The crystal growth of the single-crystalline samples of $BaCu_2V_2O_8$ was performed in a four mirror type floating-zone machine (Crystal Systems Corp., Japan) equipped with Tungsten halide lamps (Crystal Systems Corp., Japan). Since $BaCu_2V_2O_8$ is known to decompose around 770 °C close to the melting temperature [24], crystal growth was done by the traveling-solvent-floating-zone technique using a small amount (0.5 gm) of off-stoichiometric solvent having 5 mol.% excess V_2O_5, prepared by solid-state reactions as for feed rod. Growth was performed in ambient air atmosphere at a speed of 0.2 mm/h. The as-grown single crystal was about 4.5 cm in length and about 5.5 mm in diameter. After growth, a small piece of the single crystal was ground and checked with x-ray powder diffraction (Brucker D8) for phase purity. The single crystallinity of the sample was confirmed by systematically taking several x-ray Laue patterns from different parts of the crystal.

To explore the bulk properties of $BaCu_2V_2O_8$, static magnetic susceptibility measurements were performed on two single-crystalline samples of $BaCu_2V_2O_8$ with masses of 19.9 and 19.2 mg which were cut from different single-crystal growths. The measurements were carried out at the Core Lab for Quantum Materials, HZB, using a Physical Property Measurement System (PPMS) and were performed under a magnetic field of 1 T applied both parallel and perpendicular to the *c* axis. The data were collected at both low- (2–400 K) and high- (300–900 K using a heater stick) temperature regimes. Another measurement without the sample but with the same quantity of glue was also performed for the two temperature ranges to give an estimate of the background; this was fitted and subtracted from the data. For further analysis, the data collected in the low- and high-temperature regimes were normalized and combined by averaging over the overlapping temperature range (300–400 K).

The magnetic excitation spectra of $BaCu_2V_2O_8$ were explored using both powder and single-crystal inelastic neutron scattering techniques. Powder INS data were collected for a polycrystalline sample of $BaCu_2V_2O_8$ with a total mass of 21 g using the high count rate thermal time-of-flight spectrometer MERLIN [25] at ISIS, Rutherford Appleton Laboratory, UK. The sample was cooled to a base temperature of 5 K using a closed-cycle cryostat and the data were collected at both base and room temperatures ($T = 300$ K) to distinguish the magnetic contribution from the phonons. The Fermi chopper was operated in two different modes characterized by frequencies of 250 and 300 Hz and was phased to select neutrons with incident energies of $E_i = 36$ and 50 meV, respectively. The corresponding resolution widths at zero energy transfer were found to be 2.2 and 3.8 meV, respectively.

The single-crystal magnetic excitation spectra of $BaCu_2V_2O_8$ were explored by INS measurements performed on both the thermal triple-axis spectrometer PUMA [26] operated by the Heinz Maier-Leibnitz Zentrum, Garching, Germany, and on the high-flux thermal neutron triple-axis spectrometer IN8 at the Institut Laue-Langevin (ILL) in Grenoble, France.

For the measurements on PUMA, a single-crystal sample of $BaCu_2V_2O_8$ with a mass of 2.16 g was preoriented with the $(h, 0, l)$ scattering plane and mounted in a closed-cycle cryostat. The data were collected at a base temperature of 3.5 K using two different experimental settings. First with a double-focused pyrolytic graphite monochromator [PG (002)] together with a doubly focused PG (002) analyzer which provided a calculated resolution of 2 meV at a fixed final wave vector of $k_f = 2.662$ Å^{-1}. Then, the PG (002) monochromator was changed to the double-focused single-crystal Cu monochromator [Cu(220)] which is characterized by a calculated energy resolution value of 0.74 meV at fixed

final wave vector of $k_f = 1.97$ Å^{-1} and 0.992 meV at fixed final wave vector of $k_f = 2.662$ Å^{-1}.

A smaller crystal of $BaCu_2V_2O_8$ (from the same growth) with a mass of 1.38 g was used for the INS measurements at the IN8 instrument. The sample was preoriented with the (h, h, l) plane in the instrumental scattering plane and mounted into the small orange cryostat which allows it to be cooled down to a base temperature of $T = 1.5$ K. A bent perfect crystal silicon monochromator [bent Si (111)] was used together with a bent Si (111) analyzer operated at $k_f = 2.662$ Å^{-1} and giving an energy resolution of 1.07 meV. The main advantage of a silicon analyzer is that it has no second-order Bragg peaks which reduces the background contribution.

III. RESULTS AND ANALYSIS

A. Static susceptibility

Figure 2 shows the background-subtracted and normalized dc susceptibility data collected on a single-crystalline sample of $BaCu_2V_2O_8$ over the temperature range from 2 to 900 K. The constant magnetic field of 1 T was applied both parallel ($\chi_{H\|c}$) and perpendicular ($\chi_{H\perp c}$) to the c axis. The data reveal isotropic behavior within the whole temperature range except for the difference of the amplitudes of $\chi_{H\|c}$ and $\chi_{H\perp c}$. This difference is attributed to the anisotropy of the g factor which will be discussed below.

Both $\chi_{H\|c}$ and $\chi_{H\perp c}$ show a broad maximum in the vicinity of $T = 280$ K which is commonly observed in low-dimensional quantum magnets. Below this maximum, $\chi_{H\|c}$ and $\chi_{H\perp c}$ smoothly decrease as temperature is lowered and do not display any signatures of a phase transition. At very low temperatures ($T < 15$ K) both data sets start to increase slightly as temperature tends to zero. This behavior is associated with the paramagnetic contribution from the impurities which starts to play a role only at the lowest temperatures due to a small quantity of these impurities. Apart from this low-temperature impurity tail, $\chi_{H\|c}$ and $\chi_{H\perp c}$ tend towards to zero at zero temperature suggesting that this system has a nonmagnetic ground state and gapped magnetic excitation spectra.

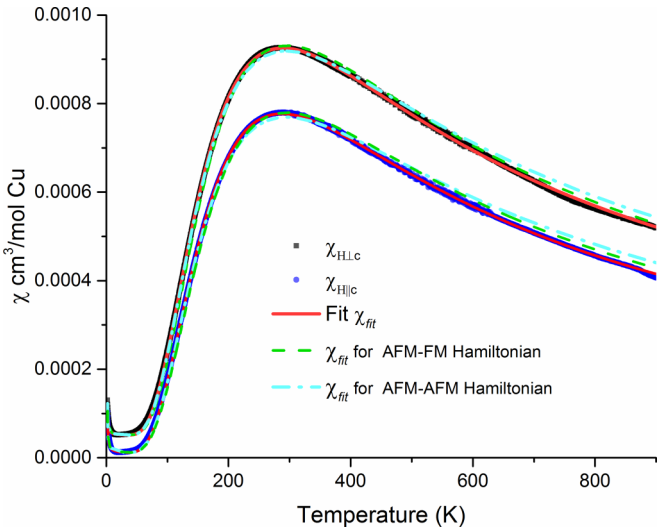

FIG. 2. Single-crystal dc susceptibility data of $BaCu_2V_2O_8$ measured under a magnetic field of $H = 1$ T applied parallel (blue dots) and perpendicular (black squares) with respect to the c axis. The solid red lines give the best fit of Eq. (2). The cyan dashed-dotted and green dashed lines correspond to fits of Eq. (2) where the magnetic exchange constants have been fixed to $J_{\text{intra}} = 40.75$ meV, $J_{\text{inter}} = 9.16$ meV and $J_{\text{intra}} = 40.92$ meV, $J_{\text{inter}} = -11.97$ meV, respectively.

Both $\chi_{H\|c}$ and $\chi_{H\perp c}$ could be fitted over the whole temperature range using the weakly coupled dimer model [27,28] and taking into account the impurity contribution as well as the diamagnetic susceptibility and van Vleck paramagnetism:

$$\chi_{\text{fit}} = \chi_0 + \chi_{VV} + \chi_{\text{imp}} + \chi_{wcd}. \quad (2)$$

Here, χ_0 and χ_{VV} describe the temperature-independent diamagnetic core susceptibility and van Vleck paramagnetism, respectively.

The χ_{imp} describes the paramagnetic Curie tail observed in the data at temperatures below 15 K which can be fitted using the Curie-Weiss law:

$$\chi_{\text{imp}} = \frac{C_{\text{imp}}}{T - \Theta_{\text{imp}}}, \quad (3)$$

where C_{imp} and Θ_{imp} are the Curie constant and Curie temperature of the impurity, respectively.

The last term χ_{wcd} represents the *weakly coupled dimer model* [27,28] which describes the magnetic susceptibility of weakly coupled dimers within mean field theory:

$$\chi_{wcd} = \frac{N_A g^2 \mu_B^2 S(S+1)/k_B T}{3 + \exp(J_{\text{intra}}/k_B T) + J_{\text{inter}}/k_B T}. \quad (4)$$

Here, N_A is Avogadro number, g is the Landé factor, μ_B is the Bohr magneton, $S = \frac{1}{2}$ is the spin value.

The weakly coupled dimer model does not assume any particular dimensionality of the magnetic system but allows J_{intra} and J_{inter} to be estimated. This model is found to be appropriate to describe the magnetic properties of $BaCu_2V_2O_8$ because the susceptibility data suggest that $BaCu_2V_2O_8$ has a gapped nonmagnetic ground state without long-range magnetic order.

The solid red lines through $\chi_{H\|c}$ and $\chi_{H\perp c}$ in Fig. 2 present the best fits which were achieved using relation (2) with the values of $J_{\text{intra}} = 39.67(7) \pm 0.003$ meV, $J_{\text{inter}} = -12.52 \pm 0.07$ meV, $g_{H\|c} = 2.09 \pm 0.03$ for $\chi_{H\|c}$ and $J_{\text{intra}} = 39.939 \pm 0.003$ meV, $J_{\text{inter}} = -7.23 \pm 0.07$ meV, $g_{H\perp c} = 2.27 \pm 0.03$ for $\chi_{H\perp c}$. The values of exchange couplings extracted from $\chi_{H\|c}$ and $\chi_{H\perp c}$ are in general agreement with each other and can be averaged to $J_{\text{intra}} = 39.80 \pm 0.13$ meV and $J_{\text{inter}} = -9.87 \pm 2.64$ meV. These results imply that $BaCu_2V_2O_8$ contains antiferromagnetic (AFM) dimers which are weakly coupled ferromagnetically (FM) with the dimerization ratio of $\alpha = -0.248$.

Anisotropy of the g factor

The values of the Landé g factor $g_{H\|c} = 2.09 \pm 0.03$ and $g_{H\perp c} = 2.27 \pm 0.03$ extracted from the fit analysis of $\chi_{H\|c}$ and $\chi_{H\perp c}$ in $BaCu_2V_2O_8$ reveal that it is anisotropic with respect to the c axis. Such anisotropy is commonly observed in copper oxides with plaquette geometry and is related to a

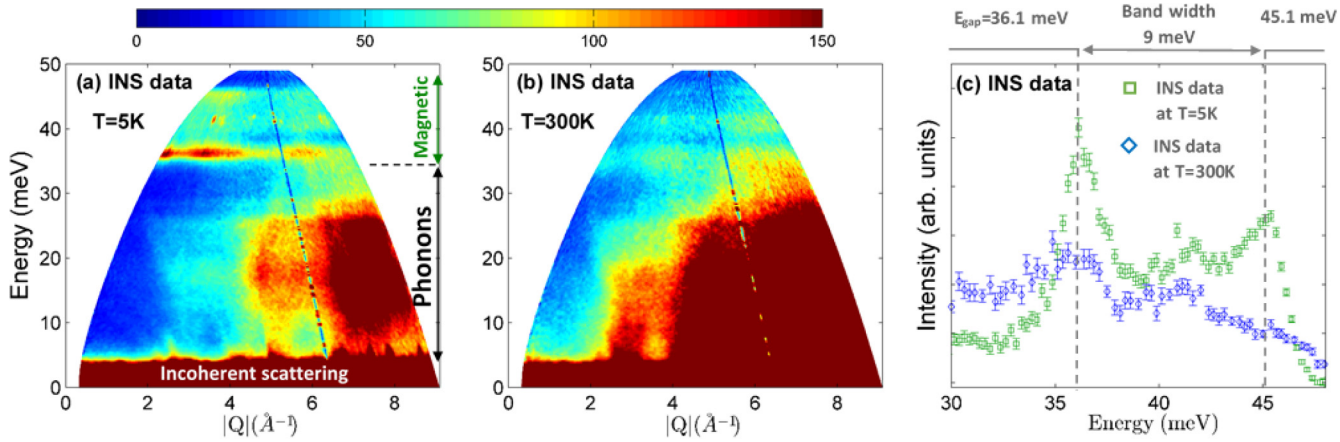

FIG. 3. INS data collected on a powder sample of $BaCu_2V_2O_8$ using the MERLIN spectrometer (a) at $T = 5$ K and (b) at $T = 300$ K with an incident neutron energy of 50 meV. (c) The energy cut through the INS data at $T = 5$ K (open green squares) and at $T = 300$ K (open blue diamonds) integrated over the wave-vector range 3.8 $Å^{-1} \leqslant |\vec{Q}| \leqslant 4$ $Å^{-1}$ and plotted as a function of the energy transfer.

strong anisotropy of the electron density distribution in the copper-oxygen plaquettes [29,30].

To be consistent with the physical origin of the anisotropy, the Landé g factor of the magnetic Cu^{2+} ions in $BaCu_2V_2O_8$ is rewritten with respect to the plane of copper-oxygen plaquettes. In $BaCu_2V_2O_8$ there are eight Cu_2O_6 double plaquettes per one unit cell where four of them contain planes perpendicular to {100} and the others contain planes perpendicular to {010}. When the magnetic field is applied parallel to the c axis it, therefore, lies within the planes of all the plaquettes so that $g_{H\|\text{plaq}} = g_{H\|c} = 2.09 \pm 0.03$. However, when the magnetic field is perpendicular to the c axis and parallel to either the a or b axis, it lies within the plaquettes which are perpendicular to either {010} or {100}, respectively, and, therefore, $g_{H\perp\text{plaq}} = 2g_{H\perp c}\text{-}g_{H\|c} = 2.45 \pm 0.03$.

The extracted values of $g_{H\|\text{plaq}} = 2.09 \pm 0.03$ and $g_{H\perp\text{plaq}} = 2.45 \pm 0.03$ are in good agreement with the values $g_{H\|\text{plaq}} \approx 2.05$–$2.11$ and $g_{H\perp\text{plaq}} \approx 2.31$ reported for the cuprates $BaCuSi_2O_6$ and $Cu(NO_3)_2 \cdot 2.5H_2O_8$ which have a similar square planar geometry [29,30]. However, they contradict the values $g_{H\|c} = 2.44$ and $g_{H\perp c} = 2.13$ reported earlier for $BaCu_2V_2O_8$ where the crystal axes appear to have been accidentally swapped [31].

B. Magnetic excitation spectrum

1. Powder inelastic neutron scattering

To get an overview of the magnetic excitation spectrum of $BaCu_2V_2O_8$, powder inelastic neutron scattering (INS) measurements were performed using the MERLIN time-of-flight spectrometer.

Figure 3(a) shows the powder INS data of $BaCu_2V_2O_8$ collected at the base temperature of $T = 5$ K and plotted as a function of wave vector ($|\vec{Q}|$) and energy (E) transfers. These data reveal that $BaCu_2V_2O_8$ has a gapped magnetic excitation band which extends over the energy range of ≈35–47 meV. The intensity of these excitations is strong at low wave vectors and decreases with increasing wave vector confirming their magnetic nature which was also verified by the comparison with the high-temperature data. Indeed, Fig. 3(b) shows the INS data collected on the same sample at $T = 300$ K which reveals that the intensity of the excitations above 30 meV decreases with increasing temperature, proving their magnetic origin. The signal below 30 meV, in contrast, becomes more intense with temperature confirming that these are phonons. The strong temperature-independent signal at low energies of 0–5 meV on both plots is incoherent elastic scattering.

Figure 3(c) shows the cuts through the INS data collected at $T = 5$ K (green squares) and $T = 300$ K (blue diamonds) integrated over the range of 3.8 $Å^{-1} \leqslant |\vec{Q}| \leqslant 4$ $Å^{-1}$ and plotted as a function of the energy transfer. The low-temperature data clarify that the magnetic excitation band extends over the range of 36.1–45.1 meV and is centered at $E_0 \approx 40.5$ meV. The bandwidth is extracted to be ≈9 meV and the ratio of the energy gap to the band width is ≈4, revealing that this is a strongly dimerized magnetic system. The high-temperature data reveal that the signal becomes weaker with increasing temperature, proving its magnetic origin.

2. Single-crystal inelastic neutron scattering

Single-crystal INS measurements of $BaCu_2V_2O_8$ were performed using the thermal neutron triple-axis spectrometer PUMA at the base temperature of $T = 3.5$ K to further explore the magnetic excitations spectrum of this compound. The measurements were performed within the $(h, 0, l)$ scattering plane either along the l or h directions to investigate the dispersion of the magnetic excitations along the main crystal axes.

Figures 4(a)–4(d) show the magnetic excitation spectra of $BaCu_2V_2O_8$ measured along the $(6, 0, l)$, $(5, 0, l)$, $(3, 0, l)$, and $(2, 0, l)$ directions, respectively. The results reveal that there are two gapped excitation branches dispersing over the energy range of ≈36–46 meV. Both modes have the same periodicity and bandwidth but are shifted with respect to each other by a half-period and alternate in intensity. Indeed, the mode, which has an intense minimum at odd l along the $(6, 0, l)$ direction becomes weaker along $(5, 0, l)$ and almost disappears along the $(3, 0, l)$ but then, strengthens along $(2, 0, l)$. The second mode which has a minimum at even l behaves the other way around.

To explore the dispersion of these modes within the (a^*b^*) plane, measurements were also performed along the $(h, 0, 5)$

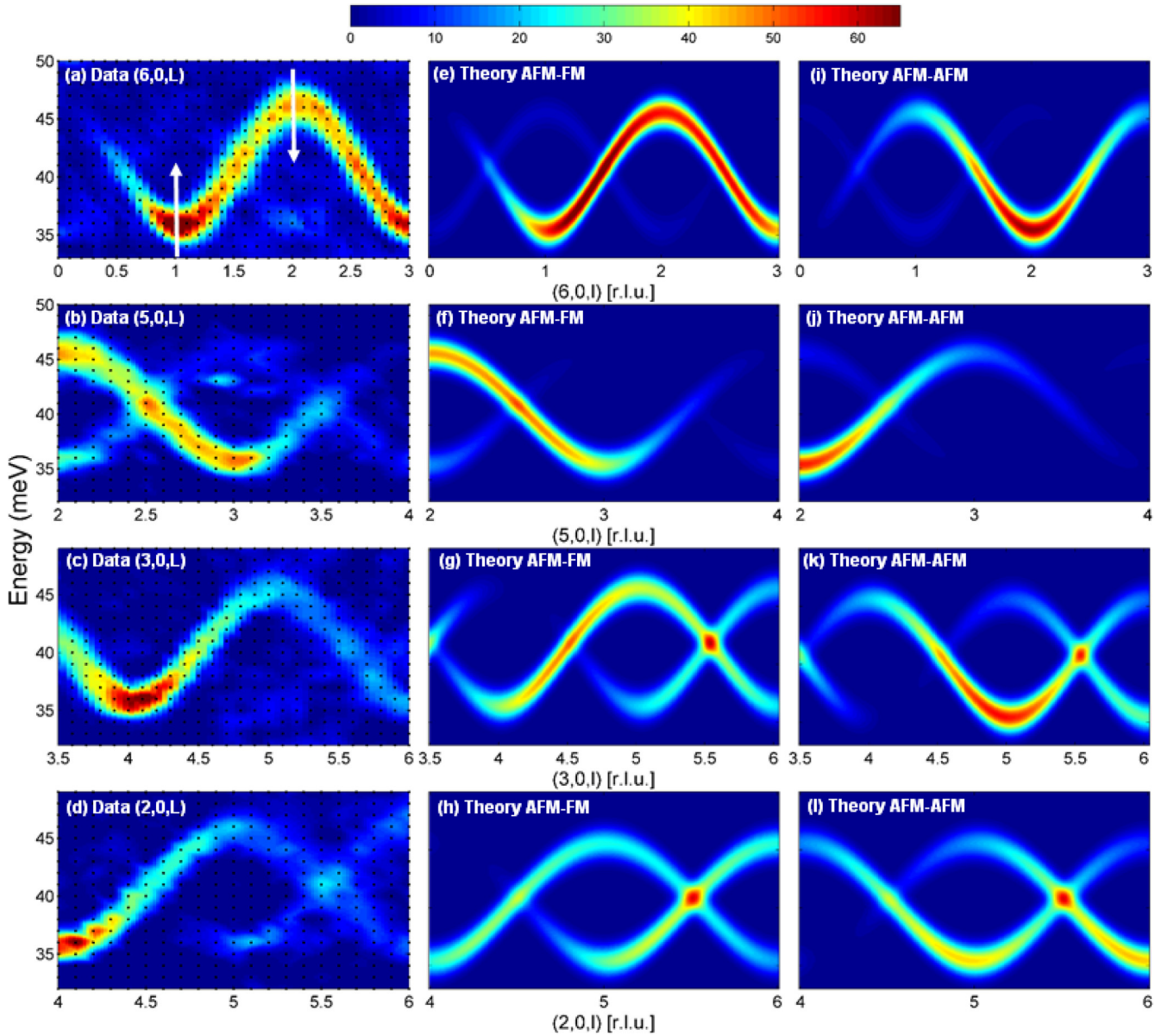

FIG. 4. Background-subtracted single-crystal INS data measured along the (a) (6, 0, l), (b) (5, 0, l), (c) (3, 0, l), (d) (2, 0, l) directions using the PUMA spectrometer at base temperature. The black dots indicate the points of measuring. The white arrows show the directions of the constant wave-vector scans measured at (6,0,1) and (6,0,2) as discussed in the text, the colors give the relative intensity. The DSF computed along the (e), (i) (6, 0, l), (f), (j) (5, 0, l), (g), (k) (3, 0, l), (h), (l) (2, 0, l) directions for AFM-FM and AFM-AFM Hamiltonian using $S_{sd}(q, \omega)$ [Eq. (7)], respectively.

and $(h, 0, 4)$ directions. Figure 5(a) shows the INS data collected along the $(h, 0, 5)$ direction which reveal that there are two flat modes at $E \approx 36$ and 46 meV whose intensities alternate along h in agreement with the data observed along the l direction. In contrast to $(h, 0, 5)$, only one mode has an intensity along the $(h, 0, 4)$ direction where h varies from $h = 0$ to 6. This is in agreement with the intensity distribution observed along $(3, 0, l)$ direction. The absence of any dispersion of the modes along the h direction implies that the coupling between the chains within the ab plane is negligible.

The observed magnetic excitation spectra suggest that $BaCu_2V_2O_8$ is a dimerised chain where dimers are coupled one dimensionally (1D) along the c axis (l direction in the reciprocal space). The fact that the two modes are identical but shifted with respect to each other by a half of period along the l direction implies that this chain is not straight and contains two dimers per magnetic unit cell giving rise to zone folding.

C. Hamiltonian of $BaCu_2V_2O_8$

To learn more about the dimer exchange path and the magnetic exchange constants, the magnetic excitation spectra of $BaCu_2V_2O_8$ were analyzed using the fifth-order expansion of the one-magnon dispersion relation $\omega(q_{h,k,l})$ proposed in the literature for the dimerized chain [7]:

$$\omega(q_{h,k,l}) = J_{\text{intra}} \sum_{n=0}^{5} a_n(\alpha) \cos(n q_l D). \tag{5}$$

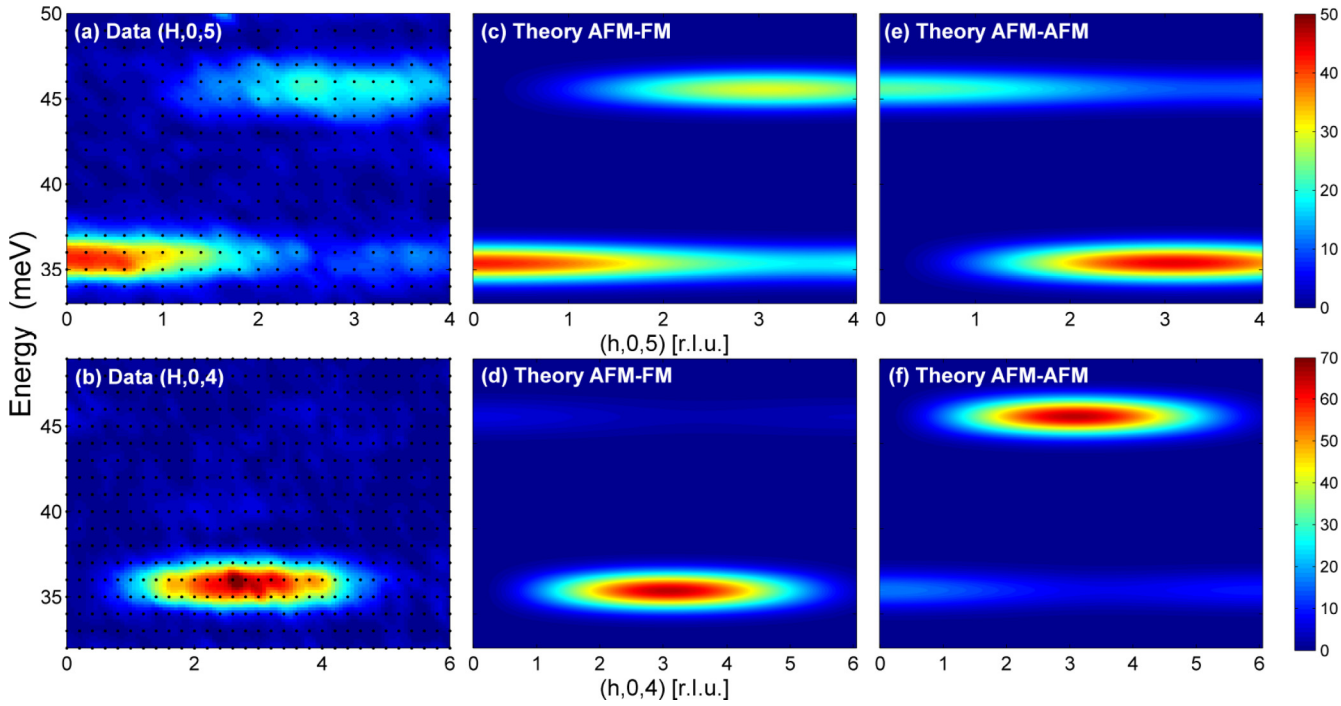

FIG. 5. Background-subtracted single-crystal INS data measured along the (a) $(h, 0, 5)$, (b) $(h, 0, 4)$ directions using PUMA spectrometer at base temperature. The black dots indicate the points that were measured and the colors give the relative intensity. The DSF computed along the (c), (e) $(h, 0, 5)$, (d), (f) $(h, 0, 4)$ directions for AFM-FM and AFM-AFM Hamiltonian using $S_{sd}(q, \omega)$ [Eq. (7)], respectively.

Here, $q_l = \frac{2\pi l}{c}$ is the wave-vector transfer along the chain direction which is the l direction for $BaCu_2V_2O_8$; D is the separation between dimers along the c axis; n is the integer of the expansion and the coefficients a_n are [7]

$$\begin{aligned} a_0 &= 1 - \tfrac{1}{16}\alpha^2 + \tfrac{3}{64}\alpha^3 + \tfrac{23}{1024}\alpha^4 + \tfrac{3}{256}\alpha^5, \\ a_1 &= -\tfrac{1}{2}\alpha - \tfrac{1}{4}\alpha^2 + \tfrac{1}{32}\alpha^3 + \tfrac{5}{256}\alpha^4 - \tfrac{35}{2048}\alpha^5, \\ a_2 &= -\tfrac{1}{16}\alpha^2 - \tfrac{1}{32}\alpha^3 - \tfrac{15}{512}\alpha^4 - \tfrac{283}{18432}\alpha^5, \\ a_3 &= -\tfrac{1}{64}\alpha^3 - \tfrac{1}{48}\alpha^4 - \tfrac{9}{1024}\alpha^5, \\ a_4 &= -\tfrac{5}{1024}\alpha^4 - \tfrac{67}{9216}\alpha^5, \\ a_5 &= -\tfrac{7}{4096}\alpha^5. \end{aligned} \tag{6}$$

The comparison of the energy dispersion observed in the magnetic excitation spectra of $BaCu_2V_2O_8$ along the l direction with $\omega(q)$ can be used to obtain D. Indeed, the INS data collected along the $(6, 0, l)$, $(5, 0, l)$, $(3, 0, l)$, $(2, 0, l)$ directions show that each mode disperses along l with a periodicity of $P = 2$ r.l.u. At the same time, the first nonconstant term in the expansion (5) suggests that the period of the dispersion in the dimerized chain is given by $P = \frac{2\pi c}{2\pi D}$. Thus, the dimer repeat distance is immediately found to be half of the c-lattice parameter.

The extracted value of $D = \frac{c}{2}$ implies that there are two dimers per c-lattice parameter for every chain. This is only possible for *model 2* [Fig. 1(d)] where the magnetic chains are in fact the screw chains. *Model 1* in contrast gives rise to linear chains where there is only one dimer per c-lattice parameter [Fig. 1(c)].

Model 2 suggests that the magnetic exchange couplings are realized via the J_2 path within the double plaquettes and the J_3 path between the plaquettes. These two exchange paths form screw chain by alternating twice along the c axis within one crystallographic unit cell leading to a reduction of the Brillouin zone by a factor of 2 along the l direction and the appearance of the second mode in the excitation spectrum.

The presence of two modes can be demonstrated by calculating the dynamical structure factor (DSF) for the magnetic screw chains using the method outlined in Ref. [32] and taking into account that the chains are dimerized. Using the mathematical transformations described in Appendix A, the DSF $[S_{sd}(q, \omega)]$ for the unit cell of $BaCu_2V_2O_8$ is given by

$$\begin{aligned} S_{sd}(q_{h,k,l}, \omega) = \{&[\cos^2(\psi_1) + \cos^2(\psi_2)]S_d(q_l, \omega) \\ &+ [\sin^2(\psi_1) + \sin^2(\psi_2)] \\ &\times S_d(q_{l+1}, \omega)\}|F_{\text{anis}}(q_{h,k,l})|^2 \end{aligned} \tag{7}$$

with

$$\psi_1 = q_h \Delta_{2(3)}; \quad \psi_2 = q_k \Delta_{2(3)}, \tag{8}$$

where ω is the frequency and $q_{h,k,l}$ is the wave-vector transfer, $\Delta_{2(3)} \approx 0.09a$ $(0.075a)$ is the displacement of the center of the dominant magnetic exchange path which can either be J_2 or J_3 along the a and b axes, with respect to the screw axis. The value of $F_{\text{anis}}(q_{h,k,l})$ is the anisotropic magnetic form factor which takes into account the oxygen plaquette surrounding each magnetic Cu^{2+} ion and is given in Appendix B. The value of $S_d(q, \omega)$ is the DSF of a single linear dimerized chain given by [7]

$$\begin{aligned} S_d(q_{h,k,l}, \omega) = [1 - \cos(q_l d_{2c(3c)})]&\Big(1 + \frac{\alpha}{2}\cos(q_l D)\Big) \\ &\times \delta(\omega - \omega(q_{h,k,l})), \end{aligned} \tag{9}$$

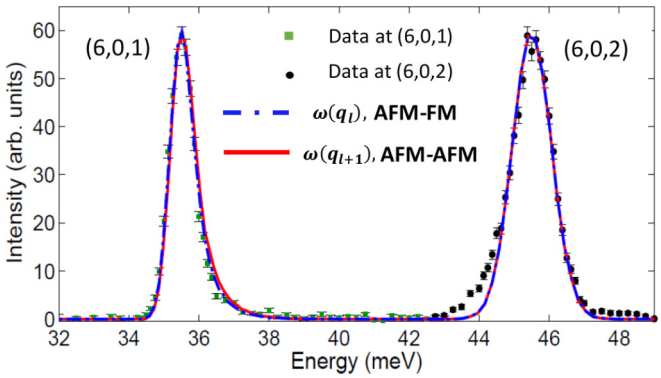

FIG. 6. Background-subtracted constant wave-vector scans measured on PUMA at (6,0,1) and (6,0,2) are given by the filled green squares and black circles, respectively. The dashed-dotted blue and solid red lines represent the result of fitting the $\omega(q_l)$ and $\omega(q_{l+1})$ one-magnon dispersion relations, which yield the AFM-FM ($J_{\text{intra}} = 40.92$ meV, $\alpha_{\text{FM}} = -0.2925$) and the AFM-AFM ($J_{\text{intra}} = 40.75$ meV, $\alpha_{\text{AFM}} = 0.225$) solutions, respectively. The peak at (6,0,2) is broader than the peak at (6,0,1) due to the different instrument settings of these two measurements.

where $d_{2c(3c)}$ is the projection of the dominant magnetic exchange path onto the c axis which equals $d_{2c(3c)} = 2.118$ Å (1.944 Å).

The $S_{sd}(q_{h,k,l}, \omega)$ [Eq. (7)] derived for *model 2* suggests that there are two nondegenerate modes $\omega(q_l)$ and $\omega(q_{l+1})$ which disperse along the l direction and are shifted by one reciprocal lattice parameter with respect to each other as observed experimentally. However, it is uncertain which mode in the INS data should be assigned to the $\omega(q_l)$ dispersion relation and which to $\omega(q_{l+1})$.

To extract the values of J_{intra} and α, the energy scans at the dispersion minimum and the dispersion maximum of the same mode were analyzed using both $\omega(q_l)$ and $\omega(q_{l+1})$ giving two sets of the solutions. Figure 6 shows the constant wave-vector scans collected at the dispersion minimum (6,0,1) and maximum (6,0,2) of the most intense mode along the $(6, 0, l)$ direction. The white arrows on Fig. 4(a) indicate the wave vectors of measurements. The dashed-dotted blue line in Fig. 6 gives the best fit of the INS data achieved using $\omega(q_l)$ convolved with the resolution function. The instrumental resolution function calculated by the RESCAL software [33] using the experimental settings of these particular measurements was convolved with the fitted function. The fitted parameters were extracted to be $J_{\text{intra}} = 40.92 \pm 0.02$ meV and $\alpha_{\text{FM}} = -0.2925 \pm 0.0025$, suggesting that in $BaCu_2V_2O_8$ the AFM dimers are weakly coupled by ferromagnetic (FM) interactions along the c axis; we call this the AFM-FM solution.

The solid red line through the data on the same figure presents the result using $\omega(q_{l+1})$. The parameters were found to be $J_{\text{intra}} = 40.75 \pm 0.02$ meV and $\alpha_{\text{AFM}} = 0.2250 \pm 0.0025$, suggesting that both exchange couplings in $BaCu_2V_2O_8$ are antiferromagnetic and this is called the AFM-AFM solution. Both solutions fit the experimental data equally well and neither solution is preferred.

Both the AFM-FM ($J_{\text{intra}} = 40.92$ meV, $\alpha_{\text{FM}} = -0.2925$) and AFM-AFM ($J_{\text{intra}} = 40.75$ meV, $\alpha_{\text{AFM}} = 0.225$) solutions were compared with the results of fitting of the dc susceptibility, $\chi_{H\|c}$ and $\chi_{H\perp c}$. Only the AFM-FM solution is consistent with the values $J_{\text{intra}} = 39.80$ meV and $\alpha_{\text{FM}} = -0.248$ extracted from the dc susceptibility data implying that the interdimer magnetic exchange coupling in $BaCu_2V_2O_8$ is ferromagnetic. Moreover, the simulations of $\chi_{H\|c}$ and $\chi_{H\perp c}$ performed using the weakly coupled dimer model keeping the interactions fixed for the AFM-FM solution, $J_{\text{intra}} = 40.92$ meV and $\alpha_{\text{FM}} = -0.2925$ (green dashed line in Fig. 2) reveal slightly better agreement with the experimental data than the simulation performed with the magnetic exchange constants fixed to the AFM-AFM solution $J_{\text{intra}} = 40.75$ meV and $\alpha_{\text{AFM}} = 0.225$ (cyan dashed-dotted line in Fig. 2).

To provide further confirmation of the Hamiltonian of $BaCu_2V_2O_8$, the DSF $S_{sd}(q, \omega)$ was computed using Eq. (7) for both the AFM-FM and AFM-AFM solutions assuming that J_3 is the dominant magnetic exchange path.

Figures 4(e)–4(h) and 4(i)–4(l) show the magnetic excitation spectrum of $BaCu_2V_2O_8$ computed along the $(6, 0, l)$, $(5, 0, l)$, $(3, 0, l)$, and $(2, 0, l)$ directions for AFM-FM and AFM-AFM solutions, respectively. The comparison of the simulations with the experimental data reveal that only the AFM-FM solution reproduces the intensity distribution correctly. Indeed, the DSF computed for the AFM-AFM Hamiltonian displays an opposite intensity distribution with respect to that observed. This result was confirmed by the simulations performed along the $(h,0,4)$ and $(h,0,5)$ directions using $S_{sd}(q, \omega)$ for both AFM-FM and AFM-AFM models (Fig. 5).

Unfortunately, due to the small difference between Δ_3 and Δ_2, switching the dominant exchange path from J_3 to J_2 in $S_{sd}(q, \omega)$ [Eq. (7))] does not change the DSF significantly, and therefore, cannot be used to determine which path gives the dominant antiferromagnetic interaction.

To identify which magnetic exchange path J_2 or J_3 is responsible for the dominant dimer exchange interaction J_{intra}, the intensity distribution of the INS data was analyzed using the first moment sum rule:

$$\begin{aligned}\hbar\langle\omega\rangle_Q &\equiv \hbar^2 \int_{-\infty}^{+\infty} \omega S(q,\omega) d\omega \\ &\propto -\sum_{m=1,2,3} |F_{\text{anis}}(q_{h,k,l})|^2 \cdot J_m \langle \mathbf{S_0} \cdot \mathbf{S_{d_m}} \rangle \\ &\quad \times [1 - \cos(\mathbf{q} \cdot \mathbf{d_m})]. \end{aligned} \tag{10}$$

Here, the contribution $J_m\langle \mathbf{S_0} \cdot \mathbf{S_{d_m}} \rangle$ is proportional to the spin-spin correlation function between two spins coupled by the magnetic exchange interaction J_m and separated by the distance d_m. Because $J_m\langle \mathbf{S_0} \cdot \mathbf{S_{d_m}} \rangle$ is modulated by a particular periodicity $[1 - \cos(\mathbf{q} \cdot \mathbf{d_m})]$ there is a link between the first moment of the DSF and the relevant Cu^{2+}-Cu^{2+} distances within the crystal structure. Therefore, fitting the experimentally determined first moment to Eq. (10) should highlight the dominant exchange paths although the absolute value of the exchange interaction J_m cannot be extracted.

Figures 7(a) and 7(b) show raw INS data measured along the $(0, 0, l)$ and $(1, 1, l)$ directions at the base temperature of $T = 5$ K. These particular directions were chosen because the math is simplified for wave-vector transfers with $h = k$. Indeed, for a general wave-vector transfer, the clockwise and anticlockwise screw chains in the unit cell of $BaCu_2V_2O_8$ produce different

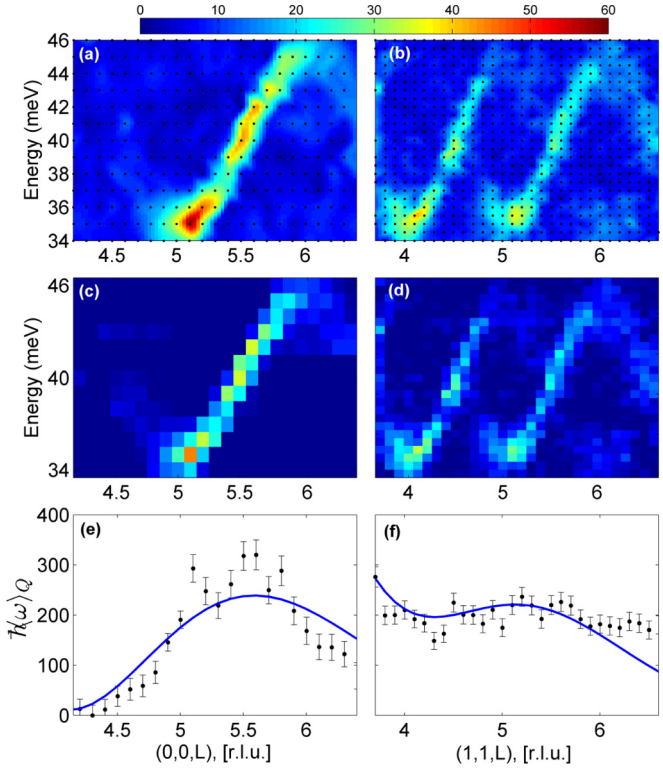

FIG. 7. (a), (b) Raw and (c), (d) background-subtracted INS data measured on the IN8 triple-axis spectrometer along the $(0, 0, l)$ and $(1, 1, l)$ directions, respectively. (e), (f) First moment of the dynamic structure factor for the $(0, 0, l)$ and $(1, 1, l)$ directions, respectively. The solid blue line through the data shows the results of fitting the relation (10) assuming two contributions from the J_2 Cu-O-Cu and J_3 Cu-O-V(II)-O-Cu paths.

modulations for the same d_m because their projections on the wave-vector transfer are different. However, for the particular case of $q_{h,h,l}$, both chains give the same modulation.

Figures 7(c) and 7(d) show the background-subtracted INS data along the $(0, 0, l)$ and $(1, 1, l)$ directions which were used to calculate the first moment of the dynamic structure factor plotted as a function of wave-vector transfer in Figs. 7(e) and 7(f), respectively. The extracted dependencies were analyzed using relation (10) counting contributions from each orientation of the J_3 and J_2 exchange paths, which are characterized by the distances $d_3 = 3.007$ Å and $d_2 = 2.87$ Å, respectively. The solid blue lines through the data on Figs. 7(e) and 7(f) show the best fit of the first moment of the DSF achieved for the values of $J_3\langle \mathbf{S_0} \cdot \mathbf{S_{d_3}}\rangle = -984 \pm 192$, $J_2\langle \mathbf{S_0} \cdot \mathbf{S_{d_2}}\rangle = -255 \pm 122$ along the (0,0,l) direction, and $J_3\langle \mathbf{S_0} \cdot \mathbf{S_{d_3}}\rangle = -769 \pm 177$, $J_2\langle \mathbf{S_0} \cdot \mathbf{S_{d_2}}\rangle = -500 \pm 163$, along the (1,1,$l$) direction. The negative sign indicates that the spin correlations agree with the proposed sign of the exchange constants and that this system is not frustrated.

For both the $(0, 0, l)$ and $(1, 1, l)$ directions, the dominant contribution arises from correlations between the spins separated by the distance d_3 which corresponds to the J_3 superexchange path. These results suggest that J_3 path is responsible for the dominant AFM J_{intra} while the weaker FM J_{inter} is realized within the double plaquettes via the J_2 path. This result is in agreement with the Goodenougth-Kanamori-Anderson rule. Indeed, the bridge angle of the Cu-O-Cu path of J_2 is 94° which is close to the crossover from AFM to FM interactions according to the Goodenough-Kanamori-Anderson rule [34–36] and is certainly consistent with the weak FM interaction observed experimentally.

IV. SUMMARY AND CONCLUSIONS

In this work, we comprehensively explored the magnetic properties of $BaCu_2V_2O_8$ at base temperature using dc susceptibility and inelastic neutron scattering. The single-crystal dc susceptibility measurements reveal that $BaCu_2V_2O_8$ has a nonmagnetic ground state suggesting that this system is dimerized. The $\chi_{H\|c}$ and $\chi_{H\perp c}$ display isotropic behavior over the whole temperature range from 2 to 900 K apart from the difference in their amplitude. This difference is attributed to the anisotropy of the g factor due to the square-planar coordination of the magnetic Cu^{2+} ions. The extracted values of $g_{H\|\text{plaq}} = 2.09 \pm 0.03$ and $g_{H\perp\text{plaq}} = 2.45 \pm 0.03$ are in good agreement with values reported for other cuprates with planar geometry [29,30].

Both $\chi_{H\|c}$ and $\chi_{H\perp c}$ were fitted well by the weakly coupled dimer model [27,28] over the whole temperature range. The extracted values of $J_{\text{intra}} = 39.80$ meV ± 0.13 meV and $J_{\text{inter}} = -9.87$ meV ± 2.64 meV imply that $BaCu_2V_2O_8$ consists of AFM dimers which are weakly coupled ferromagneticlly contradicting to all models in the literature [8,9,22,23] which assumed that both interactions are AFM.

The single-crystal INS measurements reveal that $BaCu_2V_2O_8$ has a gapped magnetic excitation spectrum which disperses over the energy range from 35.37 meV ± 0.05 meV to 45.56 meV ± 0.05 meV along the l direction but is completely dispersionless within the tetragonal plane implying a 1D coupling of the dimers along the c axis.

The observed magnetic excitation spectrum consists of two modes which are characterized by the same periodicity, size of the energy gap, and bandwidth, but are shifted with respect to each other by half a period along the l direction. The dispersion of these modes was analyzed using the fifth-order expansion of the one-magnon dispersion relation proposed for a dimerized chain [7]. The extracted dimer periodicity equals half of the unit cell which exactly corresponds to the screw-chain model [9] implying that magnetic exchange interactions in $BaCu_2V_2O_8$ are realized via the Cu-O-V(II)-O-Cu (J_3) and Cu-O-Cu (J_2) paths and form a dimerized screw chain about the c axis with two dimers per unit cell (model 2 in Fig. 1).

Two possible solutions of the Hamiltonian are given by fitting the dispersion of $BaCu_2V_2O_8$ to the dimerized chain model. The first solution suggests that both J_{inter} and J_{intra} are antiferromagnetic and equal to $J_{\text{intra}} = 40.75 \pm 0.02$ meV and $J_{\text{inter}} = 9.17 \pm 0.1$ meV. The second solution, in contrast, implies that only $J_{\text{intra}} = 40.92 \pm 0.02$ meV is antiferromagnetic while $J_{\text{inter}} = -11.97 \pm 0.1$ meV is ferromagnetic.

An analytical relation for the dynamic structure factor of the dimerized screw chain was derived to compute the magnetic excitation spectrum of $BaCu_2V_2O_8$ at base temperature. The spectrum was computed for both solutions of the Hamiltonian. The comparison with the experimental data reveals that only the AFM-FM solution ($J_{\text{intra}} = 40.92$ meV and $J_{\text{inter}} = -11.97$ meV) reproduces the observed

intensity distribution proving that the interdimer coupling is ferromagnetic.

The Cu-O-V(II)-O-Cu super-superexchange path was found to be responsible for the dominant AFM J_{intra} based on the analysis of the intensity distribution of the INS data using the first moment sum rule. A weak FM J_{inter} interaction lies within the copper-oxygen plaquettes which is consistent with the Goodenough-Kanamori-Anderson rules for superexchange coupling [34–36].

To conclude, we show that $BaCu_2V_2O_8$ is a rare physical realization of an AFM-FM dimerized chain whose magnetic energy scale is much larger than those of previously reported AFM-AFM and AFM-FM dimerized chains [3,12,13,19]. The Hamiltonian of $BaCu_2V_2O_8$ is close to being ideally one dimensional with negligible interchain coupling and was accurately solved so that the very strong antiferromagnetic and weaker ferromagnetic exchange paths were identified. Finally, the analytical relation for the dynamic structure factor of the unit cell of $BaCu_2V_2O_8$ was derived and compared to the data to verify the extracted Hamiltonian.

ACKNOWLEDGMENTS

The susceptibility measurements were performed at Core Lab for Quantum Materials, HZB. We thank K. Siemensmeyer for helping with these measurements. We also thank A. C. Tiegel, S. R. Manmana, and A. Honecker for fruitful discussions. We acknowledge the Helmholtz Gemeinschaft for funding via the Helmholtz Virtual Institute (Project No. VH-VI-521).

APPENDIX A: DYNAMIC STRUCTURE FACTOR FOR THE DIMERIZED SCREW CHAIN

This appendix describes an analytical relation for the dynamic structure factor (DSF) of the unit cell of $BaCu_2V_2O_8$ where the copper-oxygen double plaquettes, Cu_2O_6, form four dimerized screw chains along the c axis [Figs. 1(a), 1(b), and 1(d) in the main text]. Although the dynamic structure factor for the linear-dimerized chain is known [7], the DSF for the screw-dimerized chain has not been derived.

The DSF of the dimerized screw chain can be obtained using the DSF of the corresponding linear-dimerized chain [7] which has the same Hamiltonian, using the relationship between the Bravais lattice of the linear chain and the non-Bravais lattice of the screw chain where the arrangement of the magnetic sites is different [32].

Figure 8(a) shows one of the four dimerized screw chains per unit cell, formed by the J_2 (solid yellow line) and J_3 (solid double red line) magnetic exchange paths which are characterized by direct distances between the magnetic Cu^{2+} ions of $d_2 = 2.87$ Å and $d_3 = 3.077$ Å, respectively. For clarity, only the magnetic Cu^{2+} ions and their coordinating oxygen ions are shown.

Figures 8(b) and 8(c) show the projections of this chain onto the (ac) and (bc) planes illustrating two possible scenarios where either the J_2 [Fig. 8(b)] or the J_3 [Fig. 8(c)] path is responsible for the dominant antiferromagnetic intradimer exchange coupling J_{intra}. The filled green diamonds give the centers of the dimers which are shifted perpendicular to the screw axis by either $\Delta_2 = 0.09a$ or $\Delta_3 = 0.075b$ depending on whether the J_2 or J_3 path is responsible for the dominant intradimer coupling, respectively. The solid blue lines and filled blue squares give the projections of the dimers and their centers onto the screw axis and are equal to $d_{2c} = 0.26c$ if $J_2 = J_{\text{intra}}$ [Fig. 8(b)] or $d_{3c} = 0.2386c$ if $J_3 = J_{\text{intra}}$ [Fig. 8(c)]. The dashed gray lines are the projections of the weaker interdimer path onto the screw axis and are given by d_{3c} on Fig. 8(b) and d_{2c} on Fig. 8(c), respectively.

Thus, each dimerized screw chain of $BaCu_2V_2O_8$ [Fig. 8(a)] can be constructed from the dimerized linear-chain d_{2c}-d_{3c} by shifting the projections of the dimers perpendicular to the chain direction. The linear alternating-chain d_{2c}-d_{3c} lies along the screw axis and has the same exchange constants J_2 and J_3 as the d_2-d_3 dimerized screw chains. This representation can be applied to each screw chain in the unit cell of $BaCu_2V_2O_8$ [Figs. 8(e) and 8(f)].

The dimerized linear chains d_{2c}-d_{3c} form a Bravais lattice where the nodes are the centers of the dimers and edges are the screw axes which are parallel to the c axis. Assuming that both the linear d_{2c}-d_{3c} dimerized chains (Bravais lattice) and screw-dimerized chains (non-Bravais lattice) have the same Hamiltonian, the DSF of the unit cell of $BaCu_2V_2O_8$ $[S_{sd}(q,\omega)]$ can be expressed using the relationship proposed between the DSF of Bravais and non-Bravais lattices [32]:

$$S_{sd}(q_{h,k,l},\omega) = |F_{\text{anis}}(q_{h,k,l})|^2 \times \sum_{\mu=1}^{8} \left| \sum_{m=1}^{8} \exp(-i\boldsymbol{q}_{(h,k,l)} \cdot \boldsymbol{\rho}_m) \times \exp(-i\boldsymbol{T}_\mu \cdot \boldsymbol{r}_m) \right|^2 S_d(\boldsymbol{q}_{h,k,l} + \boldsymbol{T}_\mu, \omega), \tag{A1}$$

where the inner sum is taken over the magnetic sites $\vec{r}_m$ which are the centers of the dimers in the dimerized linear chains and each $\vec{r}_m$ corresponds to one of the eight magnetic sites $\vec{R}_m$ (centers of the corresponding dimers in the screw chains) within the single unit cell of $BaCu_2V_2O_8$. The relation between $\vec{r}_m$ and $\vec{R}_m$ is given by the displacement vector $\vec{\rho}_m$ so that $\vec{R}_m = \vec{r}_m + \vec{\rho}_m$ where $|\vec{\rho}_m| = \Delta_{2(3)}$ depending on which path J_2 or J_3 is responsible for J_{intra}. The outer sum is taken over all reciprocal lattice vectors T_μ of the non-Bravais unit cell of $BaCu_2V_2O_8$ within the first Brilloun zone of the Bravais unit cell.

$S_d(q_{h,k,l},\omega)$ is the DSF for the dimerized linear chain which is given by [7]

$$S_d(q_{h,k,l},\omega) = [1 - \cos(q_l d_{2c(3c)})]\left(1 + \frac{\alpha}{2}\cos(q_l D)\right) \times \delta(\omega - \omega(q_{h,k,l})), \tag{A2}$$

where $q_{h,k,l}$ is the wave-vector transfer and ω is the frequency. The energy dispersion relation $\omega(q_{h,k,l})$ for the one-dimensional dimerized chain is given in the main text [Eq. (5)] and was originally derived in Ref. [7], D is the dimer periodicity which is $D = \frac{c}{2}$ for $BaCu_2V_2O_8$.

There are eight of each of T_μ, r_m, and ρ_m which are summarized in Table I for the two scenarios $J_{\text{intra}} = J_2$ or $J_{\text{intra}} = J_3$. The substitution of the corresponding values into

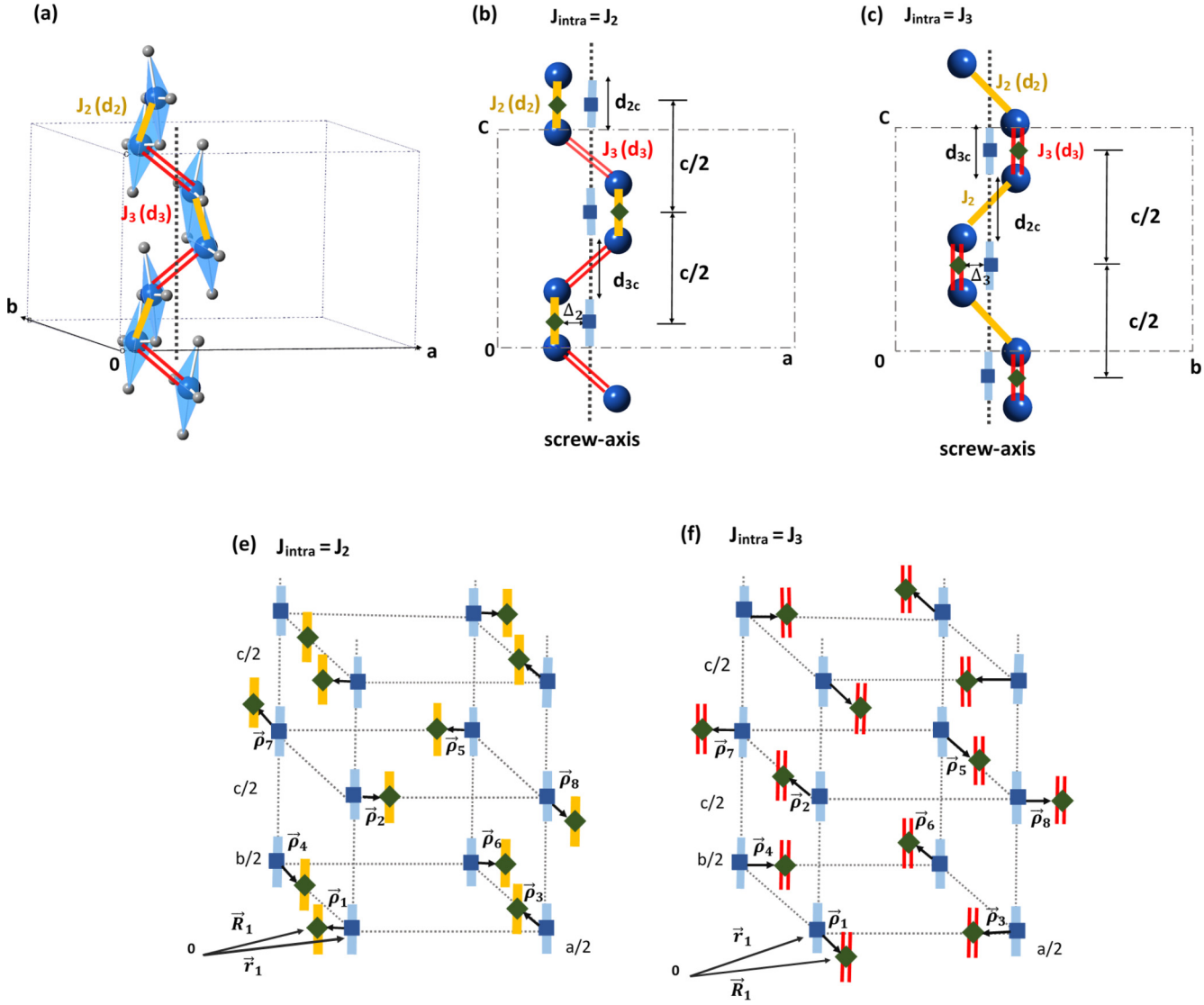

FIG. 8. (a) A single screw chain in the unit cell of $BaCu_2V_2O_8$. For clarity, only the Cu^{2+} magnetic ions (filled blue spheres) and oxygen atoms (filled gray spheres) within the plaquettes are shown. The dotted line indicates the screw axis. The solid yellow and double red lines give the magnetic exchange paths J_2 and J_3, respectively. Projection of the dimerized screw chain of $BaCu_2V_2O_8$ on (b) the ac plane illustrating the scenario where $J_2 = J_{\text{intra}}$ and on (c) the bc plane illustrating the scenario where $J_3 = J_{\text{intra}}$. The filled green diamonds give the centers of the dimers in the dimerized screw chain of $BaCu_2V_2O_8$. d_{2c} and d_{3c} are the projections of the d_2 and d_3 paths on the screw axis. The solid blue lines and filled blue squares give the projections of the dominant path (dimer) and its center on the screw axis. The Bravais unit cell of the linear chains constructed from the real unit cell of $BaCu_2V_2O_8$ where (e) $J_2 = J_{\text{intra}}$ and (f) $J_3 = J_{\text{intra}}$. The method for this construction is described in the text of Appendix A.

Eq. (A1) reveals that only T_1, T_6, T_7, and T_8 give nonzero contributions for both cases of J_{intra}.

For the case where the J_3 path is responsible for the dominant intradimer coupling J_{intra}, the DSF of $BaCu_2V_2O_8$ is given by

$$\begin{aligned} S_{sd}(q_{h,k,l},\omega) = {} & |F_{\text{anis}}(q_{h,k,l})|^2 \\ & \times (|4\cos(\psi_2) + 4\cos(\psi_1)|^2 S_d(q_{h,k,l},\omega) \\ & + |4\cos(\psi_2) - 4\cos(\psi_1)|^2 S_d(q_{h+1,k+1,l},\omega) \\ & + |4\sin(\psi_2) + 4\sin(\psi_1)|^2 S_d(q_{h,k+1,l+1},\omega) \\ & + |4\sin(\psi_2) - 4\sin(\psi_1)|^2 S_d(q_{h+1,k,l+1},\omega)), \end{aligned} \tag{A3}$$

where ψ_1 and ψ_2 equal

$$\psi_1 = q_h \Delta_3; \quad \psi_2 = q_k \Delta_3. \tag{A4}$$

For the scenario where the J_2 path is responsible for the dominant J_{intra}, the DSF is given by

$$\begin{aligned} S_{sd}(q_{h,k,l},\omega) = {} & |F_{\text{anis}}(q_{h,k,l})|^2 \\ & \times (|4\cos(\psi_2) + 4\cos(\psi_1)|^2 S_d(q_{h,k,l},\omega) \\ & + |4\cos(\psi_1) - 4\cos(\psi_2)|^2 S_d(q_{h+1,k+1,l},\omega) \\ & + |4\sin(\psi_1) - 4\sin(\psi_2)|^2 S_d(q_{h,k+1,l+1},\omega) \\ & + |4\sin(\psi_1) + 4\sin(\psi_2)|^2 S_d(q_{h+1,k,l+1},\omega)), \end{aligned} \tag{A5}$$

TABLE I. The values of the magnetic sites r_m in the Bravais lattice and their displacements ρ_m from the corresponding screw chains for the model where the dominant exchange interaction J_{intra} is assigned to the J_2 and J_3 paths, respectively. The last column gives the reciprocal vectors T_μ of the unit cell of $BaCu_2V_2O_8$ (non-Bravais unit cell).

m	r_m	ρ_m $J_{\text{intra}} = J_2$	ρ_m $J_{\text{intra}} = J_3$	μ	T_μ
1	r_1=(0,0,0)	$(-\Delta_2,0,0)$	$(0,-\Delta_3,0)$	1	(0,0,0)
					(0,0,0)
2	r_2=(0,0,1)	$(\Delta_2,0,0)$	$(0,\Delta_3,0)$	2	(0,0,1)
					$(0, 0, \frac{2\pi}{c})$
3	r_3=(1,0,0)	$(0,\Delta_2,0)$	$(-\Delta_3,0,0)$	3	(1,0,0)
					$(\frac{2\pi}{a}, 0, 0)$
4	r_4=(0,1,0)	$(0,-\Delta_2,0)$	$(\Delta_3,0,0)$	4	(0,1,0)
					$(0, \frac{2\pi}{a}, 0)$
5	r_5=(1,1,1)	$(-\Delta_2,0,0)$	$(0,-\Delta_3,0)$	5	(1,1,1)
					$(\frac{2\pi}{a}, \frac{2\pi}{a}, \frac{2\pi}{c})$
6	r_6=(1,1,0)	$(\Delta_2,0,0)$	$(0,\Delta_3,0)$	6	(1,1,0)
					$(\frac{2\pi}{a}, \frac{2\pi}{a}, 0)$
7	r_7=(0,1,1)	$(0,\Delta_2,0)$	$(-\Delta_3,0,0)$	7	(0,1,1)
					$(0, \frac{2\pi}{a}, \frac{2\pi}{a})$
8	r_8=(1,0,1)	$(0,-\Delta_2,0)$	$(\Delta_3,0,0)$	8	(1,0,1)
					$(\frac{2\pi}{a}, 0, \frac{2\pi}{a})$

where ψ_1 and ψ_2 are given by

$$\psi_1 = q_h\Delta_2; \quad \psi_2 = q_k\Delta_2. \tag{A6}$$

Because the energy dispersion for the linear dimerized chain depends only on the component of the wave-vector transfer q_l which is along the chain direction, the modes $S_d(q_{h,k,l}, \omega)$ and $S_d(q_{h+1,k+1,l}, \omega)$ which have the same q_l are degenerate as are $S_d(q_{h,k+1,l+1}, \omega)$ and $S_d(q_{h+1,k,l+1}, \omega)$.

Thus, both Eqs. (A3) and (A5) can be simplified and written in the general form

$$\begin{aligned} S_{sd}(q_{h,k,l}, \omega) = {} & |F_{\text{anis}}(q_{h,k,l})|^2 \\ & \times [[\cos(\psi_1)^2 + \cos(\psi_2)^2]S_d(q_l, \omega) \\ & + [\sin(\psi_1)^2 + \sin(\psi_2)^2]S_d(q_{l+1}, \omega)], \end{aligned} \tag{A7}$$

where

$$\begin{aligned} &\psi_1 = q_h\Delta_2; \quad \psi_2 = q_k\Delta_2 \qquad \text{for } J_2 = J_{\text{intra}}, \\ &\psi_1 = q_h\Delta_3; \quad \psi_2 = q_k\Delta_3 \qquad \text{for } J_3 = J_{\text{intra}}. \end{aligned} \tag{A8}$$

Finally, $F_{\text{anis}}(q_{h,k,l})$ is the anisotropic magnetic form factor which takes into account the planar surrounding of the magnetic copper ions and is discussed below in Appendix B.

APPENDIX B: ANISOTROPIC MAGNETIC FORM FACTOR FOR THE COPPER IONS IN THE PLANAR COORDINATION

In $BaCu_2V_2O_8$ the magnetic Cu^{2+} ions are surrounded by the O^{2-} anions forming planar copper-oxygen Cu_2O_6 double plaquettes. The magnetically active $3d_{x^2-y^2}$ electronic orbitals of Cu^{2+} lie within these double plaquettes forming strong covalent d-p bonds with the O $2p$ orbitals and the z axis is perpendicular to the plaquettes. This leads to an anisotropic magnetic form factor of the magnetic Cu^{2+} ions within the copper-oxygen double plaquettes which is given by

$$\begin{aligned} F^{\text{plaq}}(q) = {} & \langle j_0\rangle - \tfrac{5}{7}[1 - 3\cos^2(\theta)]\langle j_2\rangle \\ & + \tfrac{9}{56}\big(1 - 10\cos^2(\theta) + \tfrac{35}{4}\cos^4(\theta)\big)\langle j_4\rangle. \end{aligned} \tag{B1}$$

Here, $\langle j_0\rangle$, $\langle j_2\rangle$, and $\langle j_4\rangle$ are spherical Bessel functions and θ is the angle between the wave-vector transfer and the normal to the plaquettes [37].

In $BaCu_2V_2O_8$ the Cu_2O_6 double plaquettes have two different orientations and contain either the a-c or b-c crystal axes within the plaquette plane. Therefore, the magnetic form factor for the Cu^{2+} ions in $BaCu_2V_2O_8$ should be averaged over the two orientations of the plaquettes and is given by

$$|F_{\text{anis}}(q_{h,k,l})|^2 = \left(\frac{\left|F_1^{\text{plaq}}(q)\right|^2}{2} + \frac{\left|F_2^{\text{plaq}}(q)\right|^2}{2}\right). \tag{B2}$$

Here, the values of $F_1^{\text{plaq}}(q)$ and $F_2^{\text{plaq}}(q)$ describe the magnetic form factors of the Cu_2O_6 double plaquettes oriented perpendicular to the a and b crystal axes, respectively, and are given by Eq. (B1) with $\cos(\theta) = \frac{q_a}{|q|}$ and $\cos(\theta) = \frac{q_b}{|q|}$, respectively. Note that for wave vectors $\mathbf{q}_{h,h,l}$ with $h = k$ $F_1^{\text{plaq}}(q)$ and $F_2^{\text{plaq}}(q)$ are the same, which simplifies the expression for the anisotropic magnetic form factor $F_{\text{anis}}(q_{h,h,l})$.

[1] D. A. Tennant, C. Broholm, D. H. Reich, S. E. Nagler, G. E. Granroth, T. Barnes, K. Damle, G. Xu, Y. Chen, and B. C. Sales, Phys. Rev. B **67**, 054414 (2003).

[2] C. Rüegg, N. Cavadini, A. Furrer, H.-U. Güdel, K. Krämer, H. Mutka, A. Wildes, K. Habicht, and P. Vorderwisch, Nature (London) **423**, 62 (2003).

[3] D. A. Tennant, B. Lake, A. J. A. James, F. H. L. Essler, S. Notbohm, H.-J. Mikeska, J. Fielden, P. Kögerler, P. C. Canfield, and M. T. F. Telling, Phys. Rev. B **85**, 014402 (2012).

[4] D. L. Quintero-Castro, B. Lake, A. T. M. N. Islam, E. M. Wheeler, C. Balz, M. Månsson, K. C. Rule, S. Gvasaliya, and A. Zheludev, Phys. Rev. Lett. **109**, 127206 (2012).

[5] J. Jensen, D. L. Quintero-Castro, A. T. M. N. Islam, K. C. Rule, M. Månsson, and B. Lake, Phys. Rev. B **89**, 134407 (2014).

[6] K. P. Schmidt and G. S. Uhrig, Phys. Rev. Lett. **90**, 227204 (2003).

[7] T. Barnes, J. Riera, and D. A. Tennant, Phys. Rev. B **59**, 11384 (1999).

[8] Z. He, T. Kyômen, and M. Itoh, Phys. Rev. B **69**, 220407(R) (2004).

[9] H.-J. Koo and M.-H. Whangbo, Inorg. Chem. **45**, 4440 (2006).

[10] A. J. A. James, F. H. L. Essler, and R. M. Konik, Phys. Rev. B **78**, 094411 (2008).

[11] F. Groitl, T. Keller, K. Rolfs, D. A. Tennant, and K. Habicht, Phys. Rev. B **93**, 134404 (2016).

[12] K. Kodama, H. Harashina, H. Sasaki, M. Kato, M. Sato, K. Kakurai, and M. Nishi, J. Phys. Soc. Jpn. **68**, 237 (1999).

[13] Y. Miura, Y. Yasui, T. Moyoshi, M. Sato, and K. Kakurai, J. Phys. Soc. Jpn. **77**, 104709 (2008).
[14] M. Schmitt, O. Janson, S. Golbs, M. Schmidt, W. Schnelle, J. Richter, and H. Rosner, Phys. Rev. B **89**, 174403 (2014).
[15] H. Manaka, I. Yamada, and K. Yamaguchi, J. Phys. Soc. Jpn. **66**, 564 (1997).
[16] H. Yamaguchi, Y. Shinpuku, T. Shimokawa, K. Iwase, T. Ono, Y. Kono, S. Kittaka, T. Sakakibara, and Y. Hosokoshi, Phys. Rev. B **91**, 085117 (2015).
[17] M. Hagiwara, Y. Narumi, K. Kindo, T. Kobayashi, H. Yamakage, K. Amaya, and G. Schumauch, J. Phys. Soc. Jpn. **66**, 1792 (1997).
[18] C. P. Landee and M. M. Turnbul, Eur. J. Inorg. Chem. **2013**, 2266 (2013).
[19] M. B. Stone, W. Tian, M. D. Lumsden, G. E. Granroth, D. Mandrus, J.-H. Chung, N. Harrison, and S. E. Nagler, Phys. Rev. Lett. **99**, 087204 (2007).
[20] E. S. Klyushina, A. C. Tiegel, B. Fauseweh, A. T. M. N. Islam, J. T. Park, B. Klemke, A. Honecker, G. S. Uhrig, S. R. Manmana, and B. Lake, Phys. Rev. B **93**, 241109(R) (2016).
[21] R. Vogt and H. Müller-Buschbaum, Z. Anorg. Allg. Chem **591**, 167 (1990).
[22] S. S. Salunke, A. V. Mahajan, and I. Dasgupta, Phys. Rev. B **77**, 012410 (2008).
[23] C. S. Lue and B. X. Xie, Phys. Rev. B **72**, 052409 (2005).
[24] Z. He, T. Kyômen, and M. Itoh, J. Cryst. Growth **274**, 486 (2005).
[25] R. Bewley, R. Eccleston, K. McEwen, S. Hayden, M. Dove, S. Bennington, J. Treadgold, and R. Coleman, Phys. B (Amsterdam) **385-386**, 1029 (2006).
[26] O. Sobolev and J. T. Park, J. Large-Scale Res. Facil. **1**, A13 (2015).
[27] Y. Singh and D. C. Johnston, Phys. Rev. B **76**, 012407 (2007).
[28] D. C. Johnston, in *Handbook of Magnetic Materials*, edited by K. H. J. Buschow (Elsevier, Netherlands, 1997), Vol. 10.
[29] S. A. Zvyagin, J. Wosnitza, J. Krzystek, R. Stern, M. Jaime, Y. Sasago, and K. Uchinokura, Phys. Rev. B **73**, 094446 (2006).
[30] J. C. Bonner, S. A. Friedberg, H. Kobayashi, D. L. Meier, and H. W. J. Blöte, Phys. Rev. B **27**, 248 (1983).
[31] Z. He, T. Taniyama, and M. Itoh, J. Magn. Magn. Mater. **306**, 277 (2006).
[32] A. Zheludev, T. Masuda, I. Tsukada, Y. Uchiyama, K. Uchinokura, P. Böni, and S.-H. Lee, Phys. Rev. B **62**, 8921 (2000).
[33] D. Tennant and D. McMorrow, RESCAL for MATLAB: a computational package for calculating neutron TAS resolution functions, https://www.ill.eu/instruments-support/computing-for-science/cs-software/all-software/matlab-ill/rescal-for-matlab/.
[34] J. B. Goodenough, Phys. Rev. **117**, 1442 (1960).
[35] J. Kanamori, J. Phys. Chem. Solids **10**, 87 (1959).
[36] P. W. Anderson, Phys. Rev. **79**, 350 (1950).
[37] S. Shamoto, M. Sato, J. M. Tranquada, B. J. Sternlieb, and G. Shirane, Phys. Rev. B **48**, 13817 (1993).